

Three-dimensional crystal defect imaging by STEM depth sectioning

Ryo Ishikawa, Naoya Shibata, and Yuichi Ikuhara

Citation: Chin. Phys. B, 2024, 33 (**8**): 086101. DOI: 10.1088/1674-1056/ad4ff9

What follows is a list of articles you may be interested in

Direct observation of the distribution of impurity in phosphorous/boron co-doped Si nanocrystals

Dongke Li(李东珂), Junnan Han(韩俊楠), Teng Sun(孙腾), Jiaming Chen(陈佳明), Etienne Talbot, Rémi Demoulin, Wanghua Chen(陈王华), Xiaodong Pi(皮孝东), Jun Xu(徐骏), and Kunji Chen(陈坤基)
Chin. Phys. B, 2023, 32 (**12**): 126102. DOI: 10.1088/1674-1056/acd7cf

How to realize an ultrafast electron diffraction experiment with a terahertz pump: A theoretical study

Dan Wang(王丹), Xuan Wang(王瑄), Guoqian Liao(廖国前), Zhe Zhang(张喆), and Yutong Li(李玉同)
Chin. Phys. B, 2022, 31 (**5**): 056103. DOI: 10.1088/1674-1056/ac422d

Theoretical study on the improvement of the doping efficiency of Al in 4H-SiC by co-doping group-IVB elements

Yuanchao Huang(黄渊超), Rong Wang(王蓉), Yixiao Qian(钱怡潇), Yiqiang Zhang(张懿强), Deren Yang(杨德仁), and Xiaodong Pi(皮孝东)
Chin. Phys. B, 2022, 31 (**4**): 046104. DOI: 10.1088/1674-1056/ac20ca

Molecular dynamics simulations of dopant effectson lattice trapping of cracks in Ni matrix

Shulan Liu(刘淑兰) and Huijing Yang(杨会静)
Chin. Phys. B, 2021, 30 (**11**): 116107. DOI: 10.1088/1674-1056/ac0780

Physical properties of FePt nanocomposite doped with Ag atoms：First-principles study

Jia Yong-Fei (贾永飞), Shu Xiao-Lin (舒小林), Xie Yong (谢勇), Chen Zi-Yu (陈子瑜)
Chin. Phys. B, 2014, 23 (**7**): 076105. DOI: 10.1088/1674-1056/23/7/076105

TOPICAL REVIEW — Stephen J. Pennycook: A research life in atomic-resolution STEM and EELS

Three-dimensional crystal defect imaging by STEM depth sectioning

Ryo Ishikawa[†], Naoya Shibata, and Yuichi Ikuhara

Institute of Engineering Innovation, The University of Tokyo, Bunkyo, Tokyo 113-8656, *Japan*

(Received 22 April 2024; revised manuscript received 23 May 2024; accepted manuscript online 24 May 2024)

One of the major innovations awaiting in electron microscopy is full three-dimensional imaging at atomic resolution. Despite the success of aberration correction to deep sub-ångström lateral resolution, spatial resolution in depth is still far from atomic resolution. In scanning transmission electron microscopy (STEM), this poor depth resolution is due to the limitation of the illumination angle. To overcome this physical limitation, it is essential to implement a next-generation aberration corrector in STEM that can significantly improve the depth resolution. This review discusses the capability of depth sectioning for three-dimensional imaging combined with large-angle illumination STEM. Furthermore, the statistical analysis approach remarkably improves the depth resolution, making it possible to achieve three-dimensional atomic resolution imaging at oxide surfaces. We will also discuss the future prospects of three-dimensional imaging at atomic resolution by STEM depth sectioning.

Keywords: atomic-resolution STEM, STEM depth sectioning, depth resolution, dopants, surface topography

PACS: 61.05.J–, 68.47.Gh, 81.70.Jb, 61.72.Ff **DOI:** 10.1088/1674-1056/ad4ff9

1. Introduction

Since the successful development and implementation of geometric aberration correctors in scanning transmission electron microscopes (STEM), atomic-resolution STEM imaging and spectroscopy have become a versatile tool for nanotechnology, condensed matter physics, and materials science.[1,2] Although the first generation of geometric aberration correctors can only correct up to third-order aberrations,[3,4] electron optics have been significantly improved afterwards, and we can now partly correct 7th-order aberrations.[5,6] As the correction orders of aberrations increased, the spatial resolution in STEM gradually improved and reached 40.5 pm.[6] In addition to the improvement of spatial resolution in lateral, it should also be possible to improve the depth resolution (axial direction) because of the principles in optics:[7] the depth resolution may be given by λ/α^2, where λ is the electron wavelength, and α is the illumination semi-angle. If we have a higher depth resolution, three-dimensional objects may be imaged as a series of scanned images by gradually changing defocus along the depth direction. This methodology is known as depth sectioning, which was first proposed just after the implementation of the aberration corrector and demonstrated by Prof. Pennycook's group using annular dark-field (ADF) STEM imaging.[8,9] Although it is theoretically possible to improve the depth resolution by increasing the illumination angle, there is no experimental proof. In this review, we present our recent development of depth sectioning by large-angle illumination STEM combined with statistical analysis, and we also discuss the progress in depth resolution and the applications of depth sectioning for three-dimensional atomic-resolution STEM imaging.[10–13]

2. Depth resolution

According to the principles of optics,[7] the spatial resolution in STEM is predominantly limited by the geometric and chromatic aberrations of the entire lens system. The available α is mainly limited by geometric aberrations, and the spatial resolution of this term can be described by the Rayleigh criterion.[14] Since an electron source is energetically spread even with a cold field emission gun (FEG), the electron probe is blurred in both lateral and depth directions by chromatic aberration. With these considerations, the spatial resolution in lateral ($\Delta r_\perp$) and depth (Δr_z) directions can be given by[13]

$$\Delta r_\perp = \sqrt{(0.61\lambda/\alpha)^2 + (C_c \Delta E \alpha / E_0)^2}, \quad (1)$$

$$\Delta r_z = \sqrt{(d_0 \lambda/\alpha^2)^2 + (C_c \Delta E / E_0)^2}, \quad (2)$$

where C_c is the chromatic aberration coefficient, E_0 is the primary electron energy, and d_0 is a constant and its range is typically $1 \le d_0 \le 2$.[13] The constant d_0 depends on how the depth resolution is evaluated experimentally, including the specimen system, the STEM imaging mode, and the statistical approach.[9,15] Figure 1(a) shows the depth resolution as a function of α at the selected energy spreads of 0 eV, 0.1 eV, 0.3 eV, and 0.8 eV, where the following parameters are used with reference to the electron microscope installed at the University of Tokyo (JEM ARM300CF): E_0 is 300 keV and C_c is 1.75 mm in Refs. [12,13]. For atomic-resolution STEM imaging, α is typically 20 mrad to 30 mrad, and the theoretical depth resolution is estimated to be about 10 nm.

[†]Corresponding author. E-mail: ishikawa@sigma.t.u-tokyo.ac.jp

© 2024 Chinese Physical Society and IOP Publishing Ltd

However, with these α, the practical depth resolution is likely to be worse than 10 nm due to strong electron channeling along the atomic column. Although the depth resolution could be remarkably improved at larger α, the effect of the chromatic aberration becomes significant. With a thermal FEG ($\Delta E \sim 0.8$ eV), the depth resolution is 5 nm and is saturated at $\alpha \sim 50$ mrad. While with a cold FEG ($\Delta E \sim 0.3$ eV), the depth resolution is significantly improved to 2 nm and saturated at $\alpha \sim 70$ mrad. Figure 1(b) shows the difference in depth resolution between the selected ΔE (0.1 eV, 0.3 eV, 0.8 eV) and $\Delta E = 0$ eV, where the difference becomes larger at larger α. However, at 0.1 eV of ΔE, the depth resolution even at $\alpha \sim 100$ mrad is close enough to the ideal case of no chromatic aberration (or no energy spread). Therefore, a monochromator for an electron source ($\Delta E < 0.1$ eV)[16,17] or a chromatic aberration corrector ($C_c < 0.5$ mm).[18] becomes essential for illumination angles larger than 70 mrad.

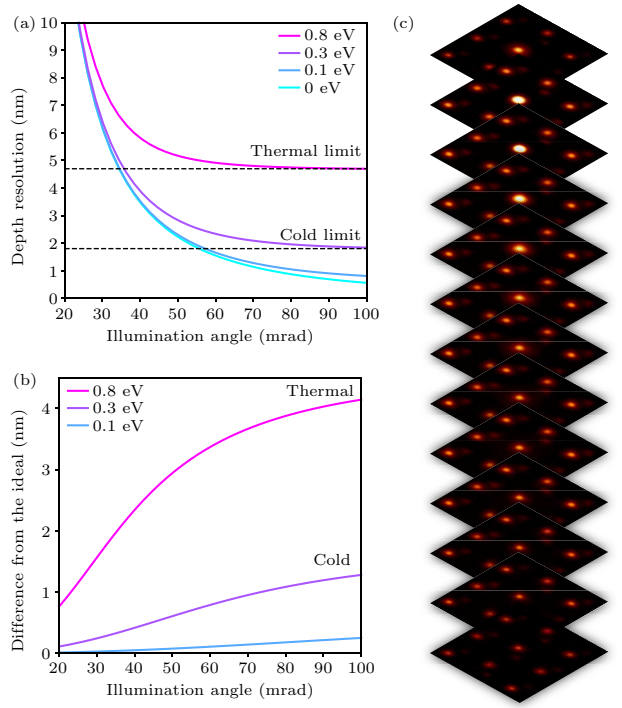


Fig. 1. (a) Depth resolution in STEM as a function of illumination angle (α), where E_0 is 300 keV, and C_c is 1.75 mm. (b) The difference of depth resolution between thermal/cold FEG and the ideal case ($\Delta E = 0$) as a function of α. (c) Schematic illustration of depth sectioning in STEM.

3. Depth sectioning

To reconstruct the 3D structure of an object, it is necessary to acquire multiple images as a 3D data set. Electron tomography is a major 3D imaging methodology in which STEM images are acquired from different orientations by mechanically rotating the object, and it has successfully reconstructed the 3D atomic structure of complex nanoparticles.[19] In depth sectioning, we acquire multiple atomic-resolution STEM images along the depth (defocus series) but in a single orientation, as shown in Fig. 1(c).[11] However, as discussed in the previous section, the depth resolution in a standard illumination angle is at most 10 nm, which is similar to the sample thickness, then it will be difficult to investigate 3D atomic structures. Therefore, it is essential to implement large-angle illumination STEM for depth sectioning. Several technical difficulties should be solved to realize STEM depth sectioning:[13] (i) distance calibration along the depth direction, (ii) minimization of mechanical instability to accurately measure a distance along the depth direction, and (iii) minimization of residual geometric aberrations to acquire atomic-resolution STEM images with larger illumination angle. To solve the first issue, we developed a high-tension focus system rather than conventional objective lens defocus. A defocus (Δf) and a high-tension variation (ΔE) have the following relationship of $\Delta f = C_c(\Delta E/E_0)$. We therefore developed precisely controllable electronics for the high-tension, and the minimum ΔE is 10 meV, which corresponds to 0.58 Å along the depth (C_c is 1.75 mm, E_0 is 300 kV). It is noteworthy that the high tension is electrostatically controllable, and therefore, we are free from magnetic hysteresis and the accompanying thermal instability of the objective lens. For the second issue, we significantly improved the microscope stability, including the water-cooling system and canceling system for external magnetic field disturbance. The in-plane sample drift for the observation (5 minutes) is 0.1 nm to 1 nm, which should be similar to the drift along the depth, and therefore the sample drift should be negligibly small. For the third issue, at larger α, it is inevitable to precisely remove residual geometric aberration. The geometric aberration correction may be minimized by the commercial software. However, the residual aberrations are still corrected by the user at the final stage. To quickly and precisely remove residual aberrations, we developed 11an automated software, where the contrast of the atomic-resolution image would be maximized.[20]

4. Demonstration of large-angle illumination STEM depth sectioning

To experimentally determine the depth resolution as a function of α, we selected the sample of Ce-doped cubic boron nitride (c-BN:Ce), where the Ce atoms are dilute doped in the c-BN bulk and exist as isolated dopants.[21] We acquired focal series ADF STEM images of c-BN:Ce viewed along the [110] axis, where the chosen illumination angles were 30 mrad, 40 mrad, 50 mrad, and 63 mrad. The focal step was 4.6 Å ($\Delta E = 80$ meV), and the image size was 512×512 pixels and 60 focal frames, covering 14 nm of the sample thickness.[13] We used 4 different sized apertures to adjust the illumination angles with the fixed condenser lens setting. To maintain the probe current at different α (11.4 ± 0.2 pA), we adjusted the extraction voltage of the electron gun in the range of 3.0 kV–3.4 kV. Figure 2(a) shows the tabulated focal series of exper-

imental ADF STEM images in which single Ce containing primitive unit cell images are aligned vertically for each α. The Ce dopants are located in the middle of the sample along the [110] direction and are visualized as bright dot contrasts. As indicated by white segments, the brighter contrast region becomes narrower with a larger α, suggesting that the depth resolution is evidently improved by a larger α. To confirm the validity of the experiments, we performed systematic image simulations using a multislice algorithm with the frozen phonon model (TEMSIM package), and the optical conditions are the same as the experiments, as shown in Fig. 2(b). Considering the following effects of (i) effective source size and (ii) chromatic aberration effect, the theoretical image simulations strongly support the experimental data. To determine the depth location of the Ce dopant and depth resolution for each 3D data set, we evaluated depth profiles as a function of defocus: (i) the mean value and (ii) the standard deviation within the region of interest (ROI), where the ROI is indicated as a white circle in Fig. 2(b). Figures 2(c) and 2(d) show the depth profiles of the mean value and the standard deviation for each α as a function of defocus. The peak positions correspond to the depth location of the Ce dopant, which is confirmed by the image simulations. With increasing α, we expected that the full width at half maximum (FWHM) of the depth profile would be narrower. However, the FWHMs are almost constant in the mean values of the depth profiles. While in the depth profile of the standard deviation, the FWHM is evidently narrowed down with the larger α, suggesting that the depth resolution is undoubtedly improved by the larger α. Here, we discuss the reason why the FWHMs are constant in the depth profile of the mean. As the first approximation, the defocused ADF STEM image could be described by a Gaussian kernel (defocused probe) convolved with the optimally focused image. In the Gaussian convolution image, the intensity is redistributed, but the mean value in the ROI is maintained. Therefore, the FWHMs are the constant in the averages of the depth profiles. However, the peak intensities are significantly reduced by the Gaussian convolution, and the intensities for all pixels around the Ce-containing atomic column become closer. Therefore, the standard deviation within the ROI has a much higher sensitivity for evaluating the depth resolution, and we would define the depth resolution for a single dopant as a 68% confidence interval in the depth profile of the standard deviation. Figure 2(e) shows the depth resolution as a function of α, where the experimental and simulated images were used for the evaluation. As expected from Eq. (2), the depth resolution is gradually improved as a function of α, and we achieved 2.14 nm depth resolution with the illumination angle of 63 mrad at 300 kV.

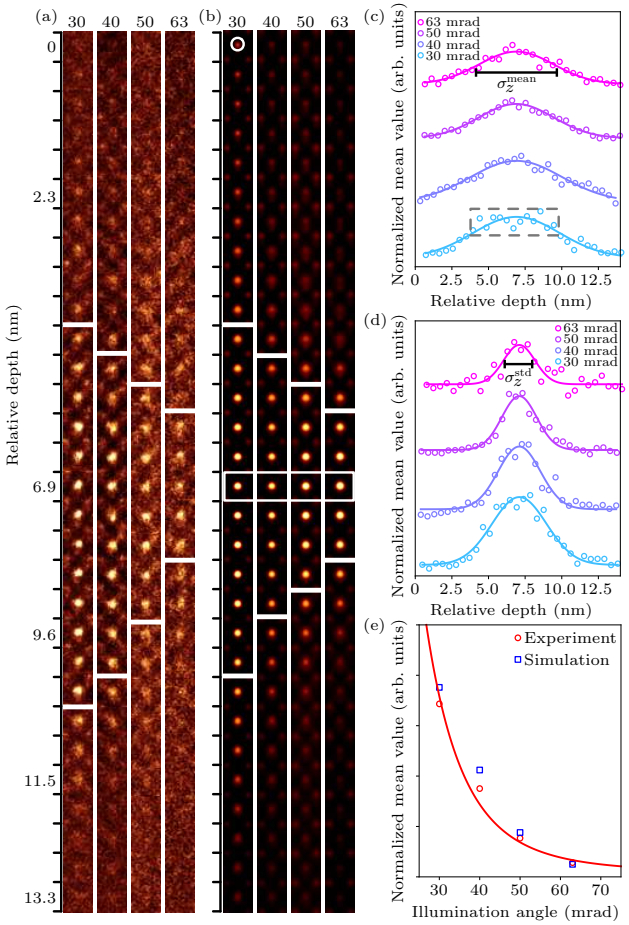


Fig. 2. (a) Experimental and (b) simulated focal series of ADF STEM images obtained from c-BN:Ce viewed along the [110] direction with the illumination angles of 30 mrad, 40 mrad, 50 mrad, and 63 mrad, respectively (left to right). Experimental depth profiles of (c) mean value and (d) standard deviation as a function of depth obtained from Ce containing N atomic columns, respectively. (e) Experimentally measured depth resolution as a function of α and the fitted curve (solid line). Adopted with permission from Ref. [13]. ©2020 American Physical Society.

5. Atomic-resolution surface imaging by STEM depth sectioning

The depth resolution has significantly improved by increasing the illumination angle. However, the achieved depth resolution is only 2.1 nm, which is far from atomic depth resolution.

It is therefore still challenging to reconstruct 3D atomic structures using depth sectioning in the bulk. However, it may still have a chance to investigate 3D atomic structure on the surface of the sample because the surface is not embedded in the bulk but the interface between a vacuum and a sample. This section will show an example of observing 3D surface topography at atomic resolution using depth sectioning combined with statistical analysis. For example, we selected strontium titanate ($SrTiO_3$) (001) surface, where the TEM sample was post-annealed at 1323 K for 10 hours to obtain an atomically flat step-terrace surface. When an electron probe is focused on the entrance surface, the Z-contrast at the atomic column could be enhanced or maximized, and we may potentially

determine the entrance surface height at the atomic level from the depth sectioning dataset. To establish a robust method for determining atomic height at the entrance surface (topography), we conducted theoretical image simulations to obtain the depth sectioning dataset as a function of specimen thickness. Figures 3(a) and 3(b) show the selected ADF STEM images as a function of defocus with different specimen thicknesses (< 25 nm) for (a) Sr atomic column and (b) Ti–O atomic column, respectively. In both cases, the Z-contrasts are maximized nearly at the entrance surface (defocus ~ 0 Å). We explored multiple statistical analyses and found that σ/μ (σ: standard deviation, μ: mean within a region of interest (ROI)) is the optimum parameter to evaluate Z-contrast. The σ/μ depth profiles of Sr atomic columns are shown in Fig. 3(a), and the contrasts are well maximized at the entrance surface (defocus $= 0$ Å) for all the specimen thicknesses. Notably, the peak position of the σ/μ depth profile is independent of the ROI size (a white circle in Fig. 3(a)). In contrast, the σ/μ depth profile of the Ti–O atomic column is maximized slightly inside the sample (defocus $= 1.95$ Å) because the TiO_2 layer is set at the subsurface in the model. These results suggest that it could be possible to determine the surface height at atomic level using the peak position of the σ/μ depth profile.

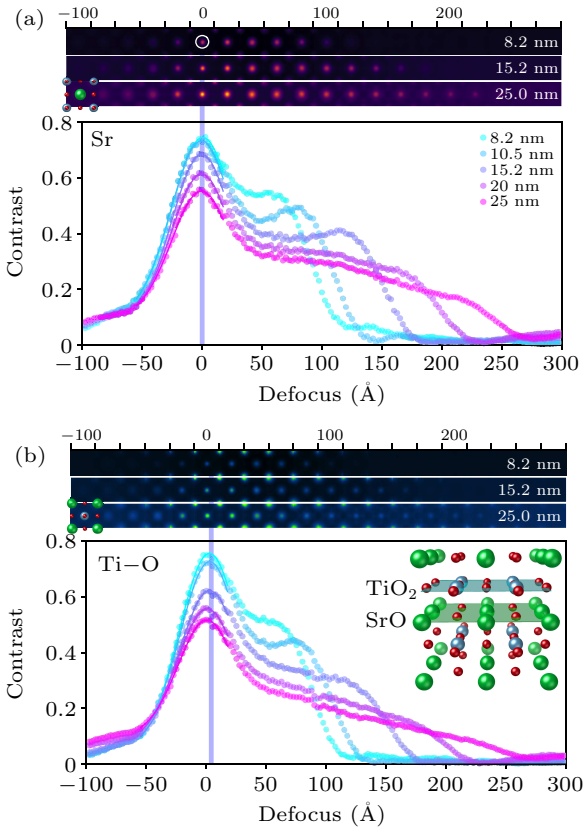


Fig. 3. Simulated focal series of ADF STEM images of $SrTiO_3$ viewed along the [001] direction and the depth profiles as a function of defocus obtained from (a) Sr and (b) Ti–O atomic columns, respectively. The specimen thicknesses are 8.2 nm, 10.5 nm, 15.2 nm, 20 nm, and 25 nm. Adopted with permission from Ref. [12]. ©2021 American Chemical Society.

To carry out surface topographic imaging at atomic resolution, we acquired a focal series of ADF STEM images of $SrTiO_3$ viewed along the [001] direction, which has 100 frames (1024×1024 pixels) with the focus step of 2.3 Å. The annealed TEM sample is clean, and hence, the sample is easy to charge during the observation because $SrTiO_3$ is an insulator. To avoid charging the sample and hydrocarbon contamination, we performed *in situ* specimen heating at 673 K in a high vacuum (8×10^{-7} Pa). Figures 4(a) and 4(b) show the low magnified and the focus averaged ADF STEM images of $SrTiO_3$, where one can see two facet planes of (100) and (110) at the sample edge. Figure 4(c) shows the selected depth profiles obtained from the atomic columns as marked by the labels a–f in Fig. 4(b). Unlike theoretical simulations, the depth profiles suffer from quantum noise because of the finite electron dose (probe current: 8.7 pA, dwell time: 4 μs/pix). To find the peak position in the depth profile, a conventional gradient descent algorithm has been used for the curve fitting. However, the gradient descent algorithm has the following issues: (i) the fitted parameter solution strongly depends on the initial values, and (ii) it is difficult to estimate the fitting error. To overcome these issues, we adopted a random walk Metropolis–Hastings (RWMH) algorithm in the Markov chain Monte Carlo method framework. In this algorithm, we first evaluate a noise variance for each depth profile and find the peak position by repeating Metropolis tests. We typically use 1100000 Metropolis tests for a single depth profile, including 100000 burn-in sweeps. Because of such large tests, we can find the optimum parameter in a large fitting parameter space. During repeating Metropolis tests, a large number of parameter candidates are generated, and the accepted parameters can also reproduce the experimental data well. Using the curve fitting method, the fitting error can be obtained simultaneously with the globally optimal solution, and the peak position (surface height) of the depth profile can be expressed as a probability density function (PDF), which is shown in Fig. 4(d). The peak position of each PDF represents the surface height, and the standard deviation represents the fitting error (standard error). For example, the labels of a and d are adjacent Sr and Ti–O atomic columns, but the overlap of the PDF profiles is small enough to show that a surface height of 2 Å can be distinguished even with the fitting error.

Figure 4(b) contains 1518 atomic columns, and the statistical distribution of the standard errors in the PDF indicates that the depth resolution at the surface is ±0.9 Å. Therefore, it becomes possible to determine the surface termination layer of either SrO or TiO_2 layers. In the present measurement, the surface height contains a standard error of ±0.9 Å. However, our sample is prepared to be atomically flat, and hence, the surface height can be classified into atomic steps. Here, we added all the PDFs of the Sr or Ti–O atomic columns, and the peaks are separated by the RWMH algorithm and classified

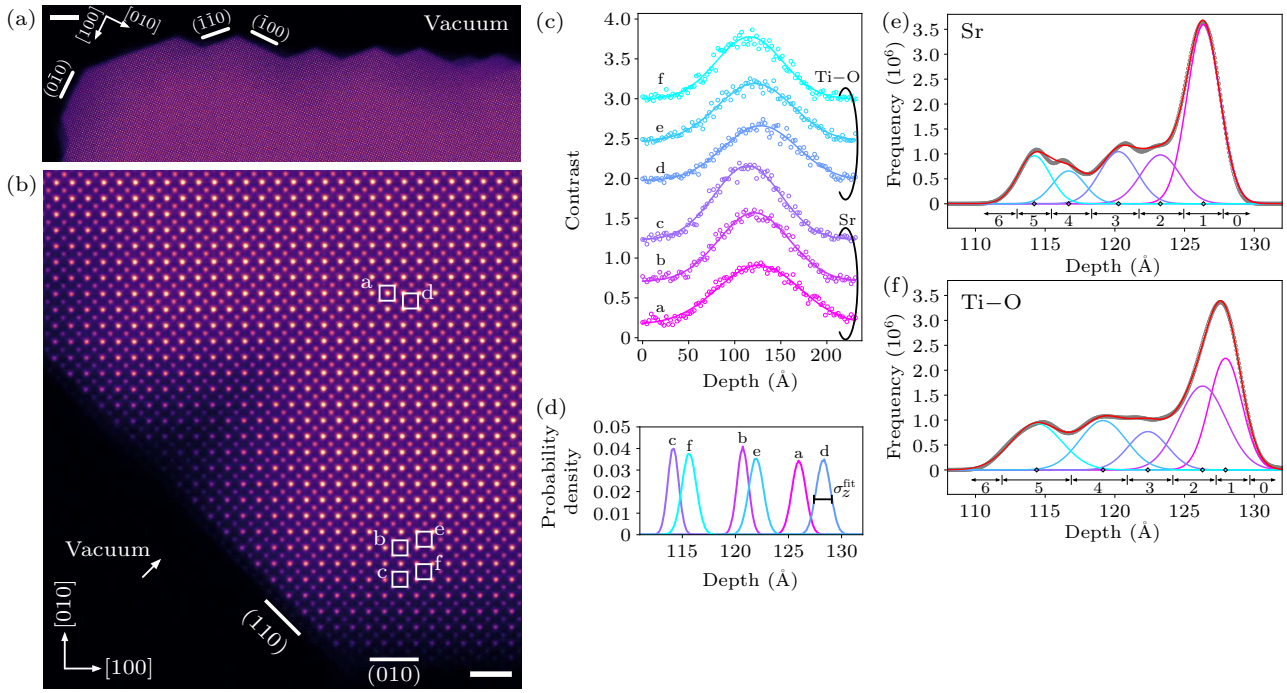


Fig. 4. (a) Atomic-resolution ADF STEM image of $SrTiO_3$ annealed at 1323 K in air. The scale bars in (a) and (b) are 5 nm and 1 nm, respectively. (c) Selected depth profiles obtained from the atomic columns labeled by a–f in panel (b). (d) The probability density function (PDF) for each atomic column. [(e) and (f)] Total PDFs for Sr and Ti–O atomic columns, respectively. Adopted with permission from Ref. [12]. ©2021 American Chemical Society.

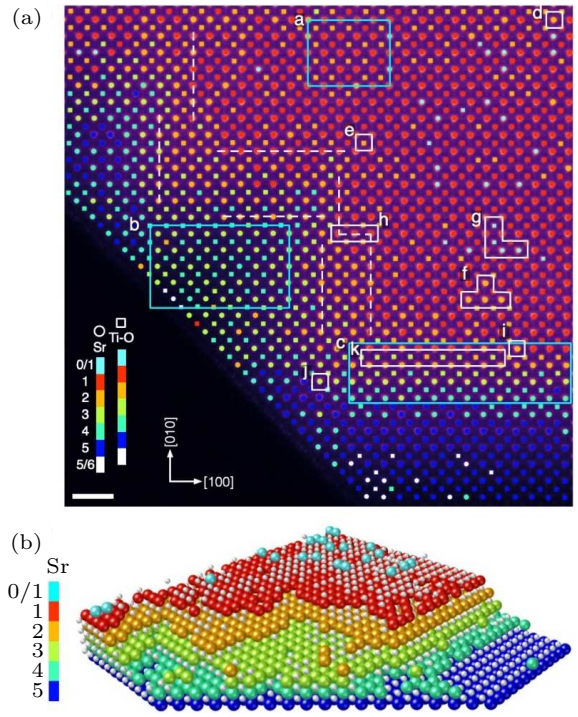


Fig. 5. (a) Reconstructed atomic surface height map. The Ti–O and Sr atomic columns are indicated by circular and square labels, respectively. The overlaid labels of a–n correspond to specific surface defects or surface termination (TiO_2 layer or SrO layer). (b) 3D reconstructed atomic surface structure model. Adopted with permission from Ref. [12]. ©2021 American Chemical Society.

into atomic surface heights (Figs. 4(e) and 4(f)). All of the atomic columns are classified into five categories, and the difference between the adjacent heights is about 4 Å. The interatomic distance along the $SrTiO_3$ [001] direction is 3.95 Å, and hence, the classified surface height should be physically correct. Figures 5(a) and 5(b) show the two-dimensional color classification and three-dimensional atomic structure model of the reconstructed surface. It reveals that the surface is formed by the step-terrace structure on the (001) surface and facets on the (100) and (110) planes. Although the majority of the topmost surface is TiO_2-termination, the narrow regions indicated by a and b have the SrO-termination. In addition, point defects such as monovacancies (V_{Sr}, V_{Ti}), vacancy clusters ($4V_{Sr}$) and adatoms are formed on the surface in d to e. These point defects are also formed at the surface step (terrace edge): h bending the step, i kink, and j step vacancy. Combining with these defects, it could be possible to form one-dimensional line defects, and we found the Ti line defect at k.

6. Conclusions and outlook

Based on the recent progress in aberration correction, we reviewed the current status and future prospects of depth sectioning. To further improve the depth resolution in STEM, it will be essential to consider the chromatic aberration correction or the smaller energy spread of the electron gun. As examples of depth sectioning, we show two applications: a proof-of-concept experiment with single Ce dopants in c-BN to measure the depth resolution, and atomic resolution surface topographic imaging by depth sectioning combined with Bayesian framework statistical analysis. The depth resolution within the sample now reaches 2.1 nm with the α of 63 mrad at 300 kV. However, at the entrance surface, it is possible to

retrieve the 3D surface atomic structure by the statistical analysis. The depth resolution in STEM is currently limited by chromatic aberration, so it is essential to develop a chromatic aberration corrector or a new cold field emission gun with a smaller energy spread. With a better electron source, it will then be important to develop a new type of geometric aberration corrector up to 100 mrad, and the depth resolution will reach the sub-nanometer scale. In addition to electron optics, it is important to improve the acquisition time because we need to acquire many STEM images as a function of defocus. Therefore, the recent development of high-speed scanning probe system could be useful to greatly reduce the overall acquisition time.[22,23] In addition, it is also important to expand the statistical analysis algorithm, which can further improve the depth resolution in STEM. By overcoming these technical difficulties, we could directly observe atom-by-atom 3D imaging using STEM depth sectioning.

Acknowledgments

We thank the collaboration with the researchers: Dr. T. Taniguchi (NIMS), Dr. K. Kawahara (Univ. Tokyo), Mr. R. Tanaka (Univ. Tokyo), and Dr. S. Morishita (JEOL Ltd.). Project supported by JST-PRESTO (Grant No. JPMJPR1871), JST-FOREST (Grant No. JPMJFR2033), JST-ERATO (Grant No. JPMJER2202), KAKENHI JSPS (Grant Nos. JP19H05788, JP21H01614, and JP24H00373), and "Next Generation Electron Microscopy" social cooperation program at the University of Tokyo.

References

[1] Pennycook S J and Boatner L A 1988 *Nature* **336** 565
[2] Pennycook S J and Nellist P D 2011 *Scanning Transmission Electron Microscopy Imaging and Analysis* (Springer, New York, 2011)
[3] Haider M, Uhlemann S, Schwan E, Rose H, Kabius B and Urban K 1998 *Nature* **392** 768
[4] Krivanek O L, Dellby N and Lupini A R 1999 *Ultramicroscopy* **78** 1
[5] Sawada H, Sasaki T, Hosokawa F, Yuasa S, Terao M, Kawazoe M, Nakamichi T, Kaneyama T, Kondo Y, Kimoto K and Suenaga K 2009 *J. Electron Microsc.* **58** 341
[6] Morishita S, Ishikawa R, Kohno Y, Sawada H, Shibata N and Ikuhara Y 2018 *Microscopy* **67** 46
[7] Born M and Wolf E 1999 *Principles of Optics* (Cambridge: Cambridge University Press)
[8] van Benthem K, Lupini A R, Kim M, Baik H S, Doh S, Lee J H, Oxley M P, Findlay S D, Allen L J, Luck J T and Pennycook S J 2005 *Appl. Phys. Lett.* **87** 034104
[9] Borisevich A Y, Lupini A R and Pennycook S J 2006 *Proc. Natl. Acad. Sci. USA* **103** 3044
[10] Ishikawa R, Pennycook S J, Lupini A R, Findlay S D, Shibata N and Ikuhara Y 2016 *Appl. Phys. Lett.* **109** 163102
[11] Ishikawa R, Lupini A R, Hinuma Y and Pennycook S J 2015 *Ultramicroscopy* **151** 122
[12] Ishikawa R, Tanaka R, Kawahara K, Shibata N and Ikuhara Y 2021 *ACS Nano* **15** 9186
[13] Ishikawa R, Shibata N, Taniguchi T and Ikuhara Y 2020 *Phys. Rev. Appl.* **13** 034064
[14] Lord Rayleigh F R S 1879 *Phil. Mag.* **8** 261
[15] Ishikawa R, Morishita S, Tanigaki T, Shibata N and Ikuhara Y 2023 *Microscopy* **72** 78
[16] Krivanek O L, Lovejoy T C, Dellby N, Aoki T, Carpenter R W, Rez P, Soignard E, Zhu J, Batson P E, Lagos M J, Egerton R F and Crozier P A 2014 *Nature* **514** 209
[17] Mukai M, Kim J S, Omoto K, Sawada H, Kimura A, Ikeda A, Zhou J, Kaneyama T, Young N P, Warner J H, Nellist P D and Kirkland A I 2014 *Ultramicroscopy* **140** 37
[18] Rose H, Nejati A and Müller H 2019 *Ultramicroscopy* **203** 139
[19] Yang Y, Chen C C, Scott M C, Ophus C, Xu R, Pryor A, Wu L, Sun F, Theis W, Zhou J, Eisenbach M, Kent P R C, Sabirianov R F, Zeng H, Ercius P and Miao J 2017 *Nature* **542** 75
[20] Ishikawa R, Tanaka R, Morishita S, Kohno Y, Sawada H, Sasaki T, Ichikawa M, Hasegawa M, Shibata N and Ikuhara Y 2021 *Ultramicroscopy* **222** 113215
[21] Ishikawa R, Shibata N, Oba F, Taniguchi T, Findlay S D, Tanaka I and Ikuhara Y 2013 *Phys. Rev. Lett.* **110** 065504
[22] Ishikawa R, Jimbo Y, Terao M, Nishikawa M, Ueno Y, Morishita S, Mukai M, Shibata N and Ikuhara Y 2020 *Microscopy* **69** 240
[23] Ishikawa R, Futazuka T, Jimbo Y, Kawahara K, Shibata N and Ikuhara Y 2024 *Sci. Adv.* **10** eadk6501